Applied Physics Letters

RESEARCH ARTICLE | APRIL 16 2024

Thermodynamic stability and ionic conductivity in lithium–germanium binary system

Anastasiia V. Iosimovska ; Alexey P. Maltsev ; Ilya V. Chepkasov ; Artem R. Oganov

Appl. Phys. Lett. 124, 163904 (2024)
https://doi.org/10.1063/5.0208577

Applied Physics Letters ARTICLE pubs.aip.org/aip/apl

Thermodynamic stability and ionic conductivity in lithium–germanium binary system

Cite as: Appl. Phys. Lett. **124**, 163904 (2024); doi: 10.1063/5.0208577
Submitted: 15 March 2024 · Accepted: 2 April 2024 ·
Published Online: 16 April 2024

Anastasiia V. Iosimovska,[1] Alexey P. Maltsev,[1,a)] Ilya V. Chepkasov,[1,2,a)] and Artem R. Oganov[1,a)]

AFFILIATIONS

[1]Skolkovo Institute of Science and Technology, Bolshoy Boulevard 30, bld. 1, Moscow 121205, Russian Federation
[2]Katanov Khakas State University, 90 Lenin pr., 655017 Abakan, Russia

[a)]**Authors to whom correspondence should be addressed:** alexey.maltsev@skoltech.ru; I.Chepkasov@skoltech.ru; and A.Oganov@skoltech.ru

ABSTRACT

Lithium–germanium binary compounds are promising anode materials for secondary lithium-ion batteries due to their high capacity, low operating voltage, and high electronic conductivity of lithiated Ge. For their successful application in batteries, it is essential to know the temperature stability of different Li–Ge phases and the variation of their ionic conductivity depending on the operating temperatures of the batteries. This work aims to comprehensively study the thermodynamic stability and ionic conductivity in Li–Ge binary compounds using a combination of first-principle computations and machine-learning interatomic potentials. We calculated convex hulls of the Li–Ge system at various temperatures and a temperature–composition phase diagram was obtained, delineating stability fields of each phase. Our calculations show that at temperatures higher than 590 K, LiGe undergoes a $I4_1/a$–$P4/mmm$ transition, which leads to a change in the ionic conductivity. We show that all stable and metastable Li–Ge compounds have high ionic conductivity, but LiGe and Li_7Ge_{12} have the lowest lithium diffusion. Trajectories of diffusion and Ge arrangements depend on lithium concentration. Based on advanced theoretical approaches, this study provides insights for the development of Li–Ge materials in lithium-ion and lithium-metal battery applications.

Lithium-ion batteries (LIBs) have been extensively studied and are used in many sectors of human life.[1–3] Most of them have a graphite anode for many reasons, including low cost, high availability, nontoxicity, reversible intercalation of lithium, and low electrochemical potential. A drawback of graphite is its relatively low theoretical capacity of 372 mA h g^{-1}. Today, there is a demand to increase the energy density of lithium-ion batteries,[1] and one of the possible ways to meet this demand is to switch from graphite to other anode materials, such as Li alloys.[4,5]

Various elements have been proposed for anode applications, such as silicon,[6–8] phosphorus,[9,10] germanium,[6,11] tin,[5,12] and metals and metallic alloys.[5] Ge is one of the candidates because of its high specific capacity (1564 mA h g^{-1}, based on $Li_{17}Ge_4$), high electronic conductivity,[13] good surface stability,[13,14] and high diffusivity of Li in Ge (which is approximately 400 times that of Li in Si at room temperature).[15] Although Ge comes at a high cost, it is an abundant element, and its high price is merely a consequence of the current low demand.[16] The drawback of Ge as anode (like for P, Si, etc.) is a high volume expansion during cycling (greater than 200%); however, this problem might be overcome by microstructural modifications, such as coating with amorphous black carbon, using porous structures, or composite materials.[17–19]

Thermodynamic stability and average voltages of intermediates during the charge–discharge process are important characteristics of anode materials. A large number of compounds have been reported in a binary Li–Ge system, both experimentally and theoretically.[6,11,20–26] Tipton *et al.*[21] predicted $Li_{21}Ge_5$, $Li_{15}Ge_4$, Li_7Ge_2, Li_5Ge_2, Li_9Ge_4, and LiGe to be stable. Using DFT calculations, Morris *et al.*[6] showed that LiGe ($I4_1/a$), Li_7Ge_3 ($P32_12$), Li_5Ge_2 ($R\bar{3}m$), Li_8Ge_3 ($R\bar{3}m$), $Li_{15}Ge_4$ ($I\bar{4}3d$), and $Li_{17}Ge_4$ ($F\bar{4}3m$) are thermodynamically stable, while electrochemical voltage decreases from ∼0.52 to ∼0.07 eV; these structures were experimentally investigated using x-ray diffraction (XRD), pair distribution function (PDF), and nuclear magnetic resonance (NMR) methods.[20] DFT calculations for Li–Ge compounds were performed at 0 K, and also showed many low-energy metastable structures; one should note that not all structures predicted by Tipton *et al.*[21] or Morris *et al.*[6] using DFT matched the experiment.[20] More accurate estimations of the phase diagram might be obtained by including the entropy term into energy and using van der Waals (vdW)-corrected DFT functionals.

Another important parameter of anode materials is the ionic conductivity of lithium; however, unlike thermodynamic properties, it has been investigated to a much lesser extent. In the paper,[27] the dynamics of lithium in a silicon and germanium host was examined using DFT, and it was shown that Li diffusivity in Ge is high (D $\sim 10^{-7}$ cm^2/s) and remains almost constant with the increase in lithium concentration. Values of diffusion coefficients, ionic conductivity, and corresponding activation energies of stable and metastable structures in the binary Li–Ge system remained unexplored.

In this paper, we revise the enthalpy–composition phase diagram at finite temperatures (up to 1000 K) using vdW-corrected DFT methods and study ionic conductivity, diffusion trajectories, and activation energies of diffusion in stable and metastable Li–Ge structures using molecular dynamics (MD) simulations with machine-learning interatomic potentials (MLIP). We use moment tensor potential (MTP),[28] which has been successfully used for many applications, such as crystal structure prediction, magnetic materials, phase transitions, thermodynamics, and kinetics,[29–33] and has allowed simulating diffusion in large systems (up to several thousand atoms) for a long time (a few nanoseconds) with DFT accuracy.

Stable phases in the Li–Ge system were predicted using the first-principles evolutionary algorithm implemented in the USPEX package.[34–36] More than 100 generations of 100 structures each were calculated. The evolutionary search was combined with structure relaxations and energy calculations using the density functional theory (DFT). All DFT calculations were performed using the Vienna *Ab initio* Simulation Package.[37–40] The optB88-vdW functional was applied to take into account van der Waals interactions between atoms.[41,42] This functional is one of those that provide the best match with the experiment for the volumes and lattice constants of layered electroactive materials for lithium-ion batteries as well as for a wide range of metallic, covalent, and ionic solids.[42–44] The energy cutoff of 400 eV for the plane wave basis set with projector augmented wave (PAW method) potentials[45,46] was specified; the convergence criteria of the self-consistent field calculations were for the electronic energy and ionic forces 10^{-8} eV and 10^{-6} eV/Å, respectively. Γ-centered k-points grid with the resolution of $2\pi \times 0.1$ Å^{-1} for the Brillouin zone sampling and the first order Methfessel–Paxton smearing with $\sigma = 0.1$ eV were used. All calculations were spin-polarized.

The thermodynamic phase stability of the systems was assessed by the phase diagrams in (energy of formation–composition) coordinates (convex hulls). A convex hull was constructed between the points $(x, E_f/atom) = (0, 0)$;(1,0). Phases located on the convex hull are stable with respect to decomposition into elemental Li and Ge or other Li–Ge compounds. The energy of formation is defined as

$$\Delta E(\mathrm{Li}_x\mathrm{Ge}_y) = \frac{E(\mathrm{Li}_x\mathrm{Ge}_y) - xE(\mathrm{Li}) - yE(\mathrm{Ge})}{(x+y)}, \quad (1)$$

where, at 0 K, E is the total energy with zero-point energy (ZPE) correction and at finite temperature it is Gibbs free energy.

We used the supercell approach and the quasi-harmonic approximation, as implemented in the Phonopy package,[47,48] to calculate vibrational frequencies and the entropy contribution to the Gibbs free energy. The dynamical stability of all structures (both stable and metastable) was verified by the absence of imaginary phonon frequencies (see Figs. S2 and S3 of the supplementary material).

For two stable phases on the convex hull, $\mathrm{Li}_{n_1}\mathrm{Ge}$ and $\mathrm{Li}_{n_2}\mathrm{Ge}$ $(n_2 > n_1)$, the following reaction is assumed to occur during lithiation:

$$\mathrm{Li}_{n_1}\mathrm{Ge} + (n_2 - n_1)\mathrm{Li} \rightarrow \mathrm{Li}_{n_2}\mathrm{Ge}. \quad (2)$$

The average voltage of the structure, V, is calculated by the following formula:

$$V = -\frac{\Delta G}{q(n_2 - n_1)} = -\frac{G(\mathrm{Li}_{n_2}\mathrm{Ge}) - G(\mathrm{Li}_{n_1}\mathrm{Ge})}{q(n_2 - n_1)} + \frac{G(\mathrm{Li})}{q}, \quad (3)$$

where $G = E + pV - TS$ is the Gibbs free energy (E is the DFT total energy, pV is assumed to be small, and TS is calculated from vibrational frequencies) and $q = 1$ is the formal charge of lithium ion.

Ionic conductivity was simulated using LAMMPS code[49,50] at temperatures 300–500 K with the step of 50 K for the supercells with 2% vacancies on lithium sites. The size of the supercells was chosen so that lattice parameters were greater than 30 Å (see Table S2 of the supplementary material). Each simulation in LAMMPS was performed with an NPT ensemble and a Nose–Hoover thermostat[51,52] with a 1 fs time step for 4 ns, after preliminary heating and equilibration for 1 ns. We used moment tensor potential (MTP)[28] of the 20th level and the MLIP-3 code.[53,54] The training set for the MLIP was created based on structures from *ab initio* molecular dynamics (AIMD) trajectories and active learning (AL). The size of the supercells for AIMD and AL (see Table S2 of the supplementary material for more details) was chosen so the lattice parameters of the structures were greater than 10 Å (or close, if the supercell is too large). The final training set consists of 563 configurations. The root mean square (RMS) errors in energies per atom and forces, as predicted by the MLIP, are less than 5 meV/atom and 100 meV/Å, respectively, for the training set, and for the validation dataset, the constructed MLIP reproduced DFT data well. Detailed errors and parameters of the MLIP are shown in the supplementary material (see Tables S1 and S2 of the supplementary material, Figs. S6 and S7, and their description).

Diffusion coefficients were calculated using mean square displacements (MSD) of Li^+ cations,

$$D = \frac{1}{6}\lim_{t\to\infty}\frac{d}{dt}\frac{1}{N}\sum_{i=1}^{N}\langle|r_i(t) - r_i(0)|^2\rangle, \quad (4)$$

where N is the number of atoms in the supercell, i is the atomic number of mobile ion (Li), and $r_i(0)$ and $r_i(t)$ are the radius vectors from the host center of mass to the ith atom at time 0 and t, respectively.

Ionic conductivity of lithium was calculated using the Nernst–Einstein formula:

$$\sigma = \frac{nq^2D}{H_r k_B T}, \quad (5)$$

where n is the Li^+ ion density, q is the formal charge of the lithium ion (q = 1), k_B is the Boltzmann constant, T is temperature, and H_r is the Haven ratio (assumed to be 1).

The activation energy E_a of ionic conductivity was calculated using the Arrhenius formula:

$$\sigma = \sigma_0 \times \exp\left(\frac{-E_a}{k_B T}\right). \quad (6)$$

Before calculations of ionic conductivity in Li–Ge systems, we performed a study of known stable and metastable Li–Ge compounds. Computational databases have varying information on the stability of diverse structures. For example, in the OQMD[55,56] database, Li_5Ge_2

appears to be stable, while in the Materials Project[57] database and the AFLOW[58] database, this structure is not present at all. However, previously, it was shown by Tipton *et al.*[21] and Morris *et al.*[6] to have space group $R\bar{3}m$. In order to understand which compounds are stable, we recalculated all known Li–Ge structures and studied their thermodynamic stability. We also carried out USPEX[34–36] calculations in order to predict previously unknown Li–Ge structures.

The stability of Li–Ge compounds was analyzed by the calculation and construction of a convex hull, as shown in Fig. 1. Zero-point energy (ZPE) contribution was taken into account during the calculation of the convex hull. Seven phases on the convex hull were found to be thermodynamically stable, namely Ge–$Fd\bar{3}m$, LiGe–$I4_1/a$,[25] Li_7Ge_3–$P3_212$,[6] $Li_{13}Ge_4$–$Cmmm$, $Li_{15}Ge_4$–$I\bar{4}3d$,[59] $Li_{17}Ge_4$–$F\bar{4}3m$,[60] Li–$Im\bar{3}m$.

Tipton *et al.*[21] theoretically determined the phase of Li_5Ge_2 using the genetic algorithm for structure and phase prediction (GASP) code. In our calculations, Li_5Ge_2 is above the convex hull by 0.8 meV/atom at 0 K and 1.7 meV/atom at 300 K, but in calculations without ZPE, it is on the convex hull (see the supplementary material). $Li_{12}Ge_7$ is also close to the convex hull (2 meV/atom at 0 K and 15 meV/atom at 300 K). Morris *et al.*[6] similarly found Li_5Ge_2 and $Li_{12}Ge_7$ to be above the convex hull.

Using the USPEX calculation, we also found the stable phase $Li_{17}Ge_4$ previously revised from $Li_{22}Ge_5$ by Goward *et al.*[60] using a more accurate description of the position of lithium atoms in the structure. Li_7Ge_{12}–$P2/n$ was detected experimentally,[22] but in our calculations it is slightly above the convex hull (10 meV/atom at 0 K and 5 meV/atom at 300 K) and might be kinetically stabilized, as well as $Li_{22}Ge_5$ (21.9 meV/atom above the convex hull, see the supplementary material).

Due to the fact that these materials are used in batteries at nonzero temperature, it is important to study the phase diagram at different temperatures. For this purpose, we calculated phonon densities of states (PhDOS) for the 32 stable and low-energy metastable structures shown in Fig. 1(a). Integration over the phonon DOS allowed us to calculate the zero-point energy and vibrational contribution to the Gibbs free energy for all studied compounds and construct convex hulls at finite temperatures.

The stability of the predicted compounds at different temperatures is summarized in the composition–temperature phase diagram [Fig. 1(b)]. Our calculations show that at temperatures higher than 590 K, LiGe–$I4_1/a$ has a phase transition into the LiGe–$P4/mmm$ structure (Fig. 2). The LiGe–$P4/mmm$ structure was also predicted by USPEX calculation.

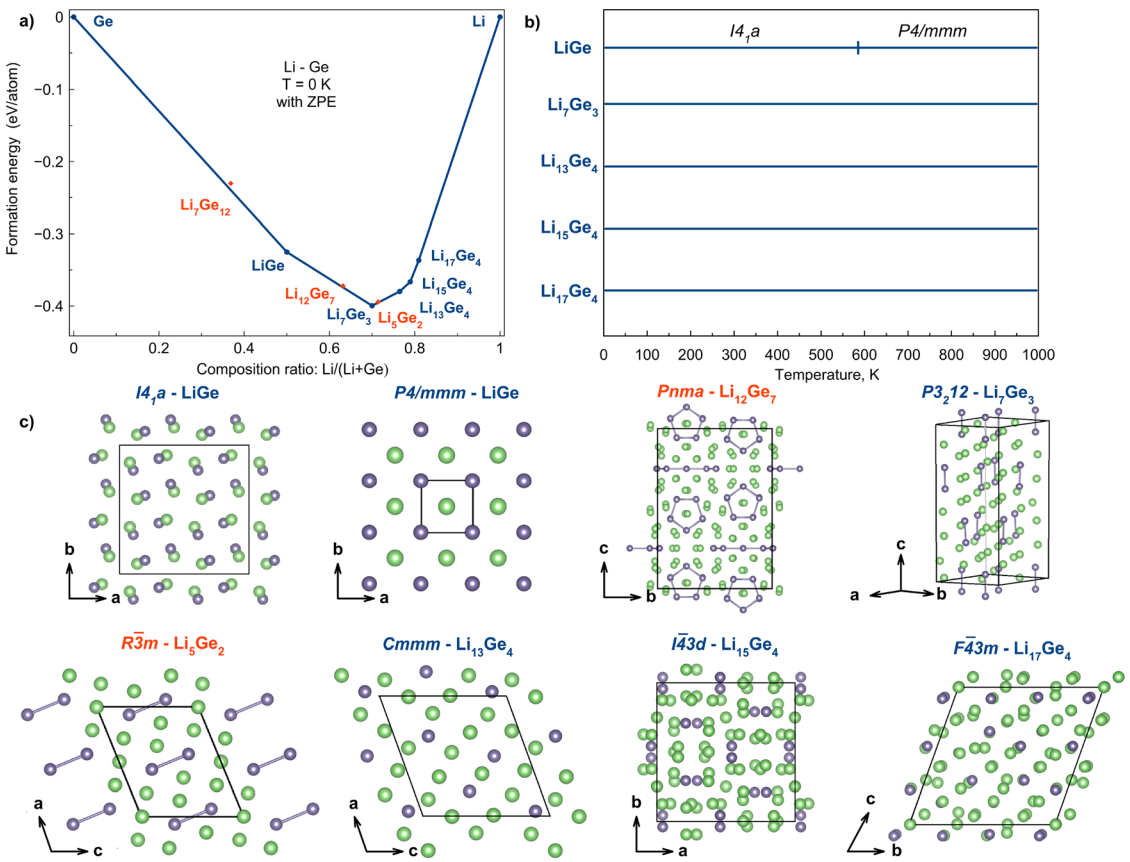

FIG. 1. (a) Calculated convex hull of the Li–Ge system at T = 0 K with ZPE. Blue circles represent stable compounds and red diamonds show metastable ones. (b) Composition–temperature phase diagram, solid lines show temperature regions where the structures are stable. (c) Crystal structures of considered Li–Ge compounds, green atoms and purple atoms are Li and Ge, respectively. Convex hull without ZPE showing a larger number of metastable structures is in the supplementary material (see Fig. S1).

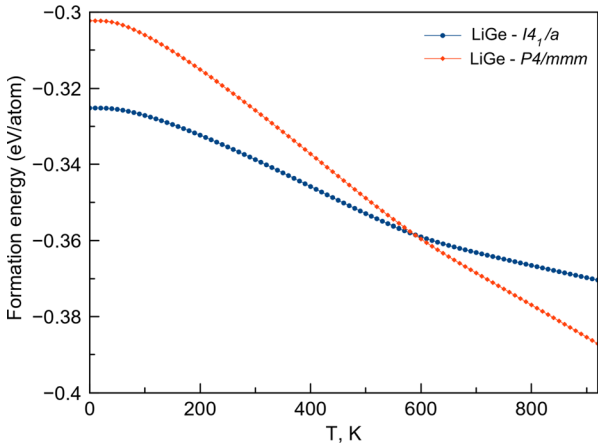

FIG. 2. Gibbs free energy of formation of LiGe phases.

The dependence of voltage on temperature is a key parameter when using anodes in fast-charging/discharging batteries. Figure 3 shows the average voltages of stable structures relative to lithium metal. At 300 K, the average potential of LiGe is 0.67 eV and the average potential of $Li_{17}Ge_4$ is 0.06 eV. With the increase in temperature, the average potential of LiGe increases and the average potential of other phases decreases.

To be used as anodes, all components of the anode must be electronic conductors; therefore, we calculated the electronic density of states for all stable and metastable Li-Ge compounds and found that all these phases there is a zero bandgap, indicating all structures are electronic conductors (see Figs. S4 and S5 of the supplementary material).

Ionic conductivity (diffusivity) is an important parameter of anode materials for fast charge and discharge, but previously it was not studied for Li–Ge stable and metastable phases. We calculated diffusion using molecular dynamics simulations and machine-learning interatomic potentials. In our previous works, this method showed results in good agreement with experiments.[9,31] Figure 4 shows the ionic conductivity of stable systems and low-lying metastable phases with 2% vacancy concentration as a function of temperature. Figure S8 (see the supplementary material) shows the diffusion trajectories of the Li ions. Most structures have high ionic conductivity of about $\sim 10^{-2}$–10^{-1} S/cm at room temperature. (One should note that molecular dynamics, in general, tends to overestimate values of diffusion coefficients and ionic conductivity at low temperatures; however, even adjusted accordingly, ionic conductivity should remain at a very high level in real systems.) Both phases of LiGe, as well as Li_9Ge_4 and Li_7Ge_{12}, are inferior in ionic conductivity to the other phases; moreover, in LiGe ($I4_1/a$), diffusion strongly depends on vacancy concentration (our calculations show there is no Li^+ self-diffusion without vacancies), and reactions involving these compounds might be the bottleneck in the overall charge–discharge rate. Li_7Ge_{12} is the only phase with a ratio of Li atoms to Ge atoms lower than 1, and because of the strong bonding of Li to the special five-membered Ge rings, there are

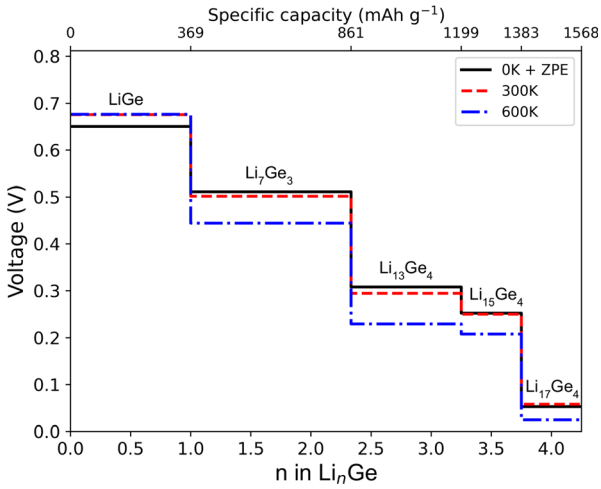

FIG. 3. Calculated average voltages relative to lithium metal for Li–Ge stable structures at 0 K (with ZPE correction), 300, and 600 K.

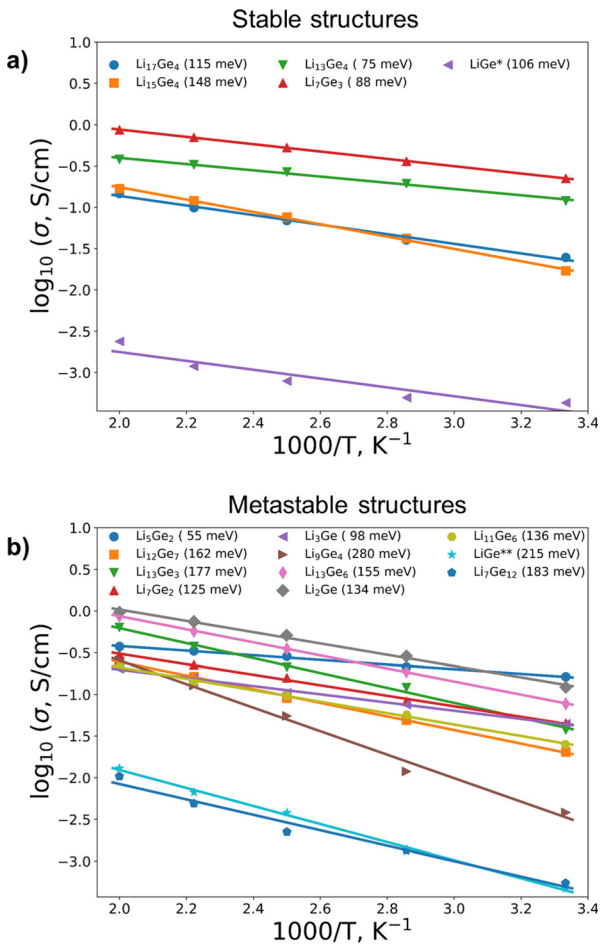

FIG. 4. Calculated ionic conductivity and activation energies (in parentheses) of stable (a) and metastable (b) Li–Ge compounds as a function of temperature. LiGe* and LiGe** are $I4_1/a$ and $P/4mmm$ phases, respectively.

fewer loosely bound mobile ions remaining, making diffusion more difficult.

Diffusion trajectories depend on Ge motifs in the crystal structure and these in turn change with Li concentration. At high lithium concentration, Ge is fully surrounded by Li and isolated from other Ge atoms ($Li_{13}Ge_3$, $Li_{17}Ge_4$, Li_4Ge, $Li_{15}Ge_4$, and Li_7Ge_2); at medium concentration, Ge form Ge–Ge dumbbells ($Li_{13}Ge_4$, Li_3Ge, Li_5Ge_2, Li_7Ge_3, Li_9Ge_4, $Li_{13}Ge_6$, Li_2Ge, and LiGe–$I4_1/a$); and at low lithium concentration, germanium starts to form five-membered rings and stars ($Li_{11}Ge_6$, $Li_{12}Ge_7$, and Li_7Ge_{12}). The bonding patterns of germanium might be described within the Zintl–Klemm concept and 8 − N rule. Pure germanium has 8 − 4 = 4 covalent bonds. Each lithium atom donates an electron, so at Li/Ge = 1, germanium imitates phosphorus, at Li/P = 2 germanium imitates sulfur, at Li/P germanium imitates halogens, and at Li/P = 4 germanium is isolated from other germanium atoms (the same patterns were obtained in a recent paper for Li–P compounds[61]). At high Li concentration (isolated Ge arrangement), the diffusion is three-dimensional. In structures with Ge dumbbells, the diffusion is also 3D, but the planes perpendicular to Ge–Ge dumbbell lines become more preferable (see the Li_5Ge_2 example in Fig. S6 of the supplementary material). Ge–Ge dumbbells are often separated by 2–7 Li atoms; closest Li atoms are strongly bonded with Ge (see the example for Li_7Ge_2 in Fig. 5) and have low diffusivity or do not diffuse at all, while weakly bonded Li atoms in between diffuse quickly even without vacancies. Diffusion in structures with Ge rings and stars becomes 2D; lithium atoms inside Ge rings are strongly bonded and do not diffuse in contrast to the outer lithium atoms closest to the rings.

To summarize, we have performed an extensive study of Li–Ge compounds using density functional theory, evolutionary structure prediction algorithms, molecular dynamics, and machine-learning approaches. Our first-principle calculations allowed us to determine the stability regions of all considered structures in the temperature range of 0–1000 K. We have found that LiGe–$I4_1/a$, Li_7Ge_3–$P3_212$, $Li_{13}Ge_4$–$Cmmm$, $Li_{15}Ge_4$–$F\bar{4}3/a$, and $Li_{17}Ge_4$–$F\bar{4}3m$ are stable at room temperature. LiGe has a phase transition from $I4_1/a$ to $P4/mmm$

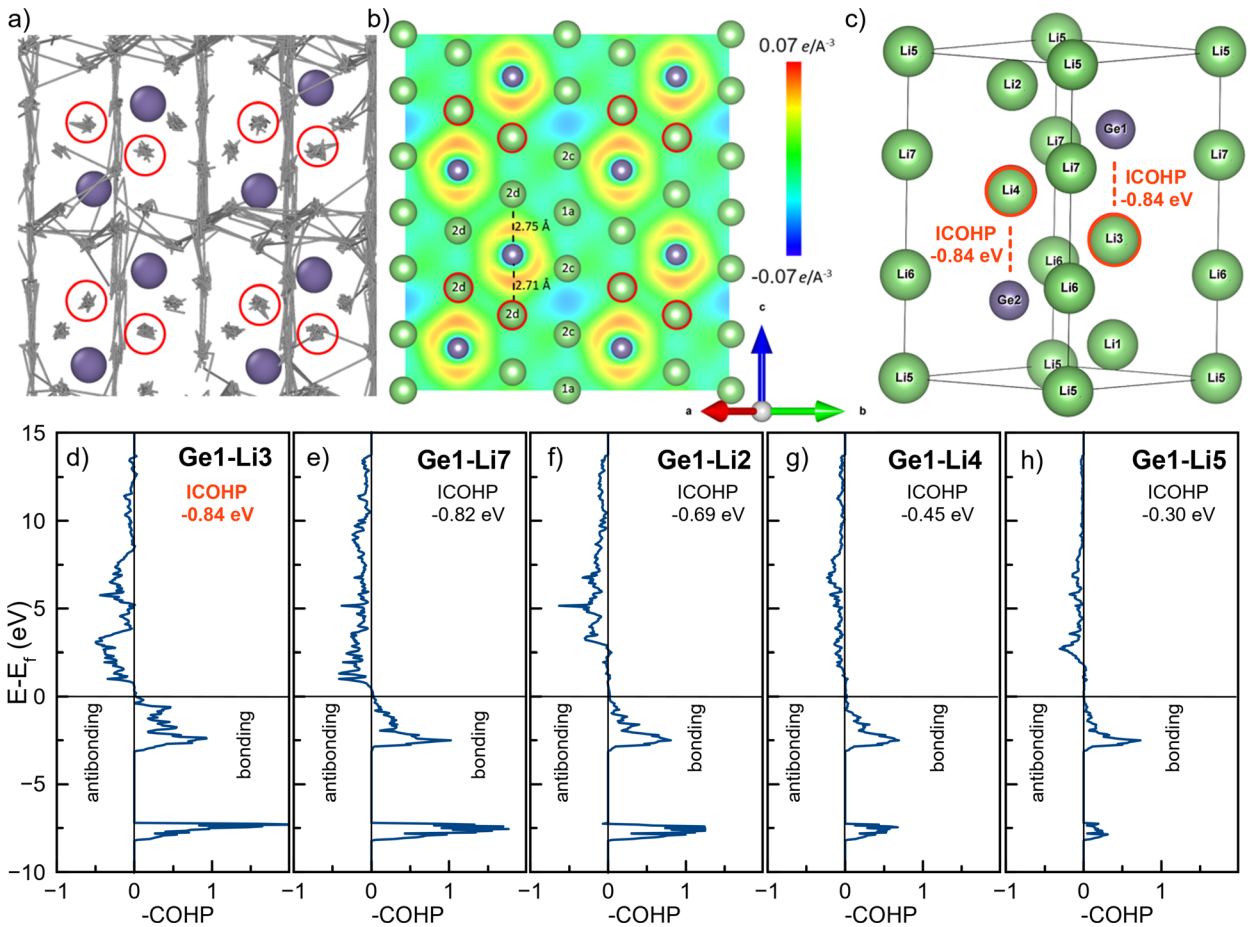

FIG. 5. (a) Calculated trajectories of Li-diffusion in Li_7Ge_2 (some additional trajectories correspond to the diffusion in parallel planes). (b) Charge difference (cross section through 110 plane) for Li_7Ge_2. Yellow and blue areas are localizations of negative and positive charge, respectively. Atoms circled in red are most strongly bound to germanium and have the lowest diffusivity. (c) Primitive cell of Li_7Ge_2. (d)–(h) COHP diagrams for the interaction between Ge atom and nearest Li atoms. The integrated COHP (ICOHP) which reflects the bond strength (the more negative value, the stronger the bond strength) was also calculated. Li atoms that do not move are most strongly bound to Ge, as can be seen from the ICOHP values (−0.84 eV). For more details about COHP calculations see the supplementary material.

structure at a temperature of 590 K. Our results indicate a variety of metastable compounds, some of which might exist at a solid electrolyte interphase during battery operation and take part in complex charge–discharge processes.

In this work, diffusion in Li–Ge binary compounds has been simulated within molecular dynamics and machine-learning interatomic potentials. We have found that most of the structures have high ionic conductivity of about $\sim 10^{-2}$–10^{-1} S/cm at room temperature. However, both phases of LiGe, as well as Li_9Ge_4 and Li_7Ge_{12}, are inferior in ionic conductivity to the other structures, and diffusion depends on the availability of vacancies; reactions with these compounds might be the limiting in lithiation/delithiation. The study of lithium diffusion paths in lithium–germanium compounds revealed that the concentration of lithium atoms in the structure determines the topology of the diffusion channel network. In high lithium concentration compounds, germanium is surrounded by lithium atoms and isolated from other germanium atoms, resulting in three-dimensional (3D) lithium diffusion. In medium concentration compounds, germanium forms two-centered Ge–Ge dumbbells, and diffusion remains 3D, but planes perpendicular to the Ge–Ge dumbbell lines become more preferred. In low lithium concentration compounds, germanium starts to form five-membered rings and stars, and diffusion becomes two-dimensional (2D), with strongly bound lithium atoms that do not diffuse in contrast to the outer lithium atoms closest to the rings. Our findings suggest that lithium–germanium compounds are promising candidates for solid-state anodes, composite anodes in lithium-ion or lithium-metal batteries, where high lithium diffusivity is essential.

See the supplementary material for details of structure prediction, the convex hull without ZPE (Fig. S1); phonon band structures and densities of states (DOS) of all stable (Fig. S2) and metastable (Fig. S3) structures; electronic DOS for stable (Fig. S4) and metastable (Fig. S5) structures; details of the machine-learning interatomic potential construction, and errors for the training and validation sets of the constructed MLIP (Table S1); details of the structure of supercells, taken for the training of the MLIP and MD simulations (Table S2); energy and force errors in the validation dataset and their distributions (Figs. S5 and S6); trajectories of diffusion of stable and metastable structures (Fig. S7); and details of COHP calculations.

The study was supported by the Russian Science Foundation. DFT calculations of structural stability were supported by Grant No. 19-72-30043 and calculations of the ionic conductivity were supported by Grant No. 22-73-00219. The calculations were carried out using the resources of the Center for the Information and Computing of the Research Center for Information and Computational Technologies at Novosibirsk State University and the Arkuda supercomputers at Skoltech.

AUTHOR DECLARATIONS

Conflict of Interest

The authors have no conflicts to disclose.

Author Contributions

Anastasiia V. Iosimovska: Formal analysis (equal); Visualization (equal); Writing—original draft (equal). **Alexey P. Maltsev:** Formal analysis (equal); Methodology (equal); Visualization (equal). **Ilya V. Chepkasov:** Conceptualization (equal); Visualization (equal); Writing—original draft (equal). **Artem R. Oganov:** Supervision (equal); Writing—review & editing (equal).

DATA AVAILABILITY

The data that support the findings of this study are available from the corresponding authors upon reasonable request.

REFERENCES

[1]J. B. Goodenough and Y. Kim, "Challenges for rechargeable Li batteries," Chem. Mater. **22**, 587–603 (2010).
[2]J.-M. Tarascon and M. Armand, "Issues and challenges facing rechargeable lithium batteries," Nature **414**, 359–367 (2001).
[3]B. Scrosati and J. Garche, "Lithium batteries: Status, prospects and future," J. Power Sources **195**, 2419–2430 (2010).
[4]N. Nitta and G. Yushin, "High-capacity anode materials for lithium-ion batteries: Choice of elements and structures for active particles," Part. Part. Syst. Charact. **31**, 317–336 (2014).
[5]X. Gu, J. Dong, and C. Lai, "Li-containing alloys beneficial for stabilizing lithium anode: A review," Eng. Rep. **3**, e12339 (2021).
[6]A. J. Morris, C. Grey, and C. J. Pickard, "Thermodynamically stable lithium silicides and germanides from density functional theory calculations," Phys. Rev. B **90**, 054111 (2014).
[7]L. Lin, X. Xu, C. Chu, M. K. Majeed, and J. Yang, "Mesoporous amorphous silicon: A simple synthesis of a high-rate and long-life anode material for lithium-ion batteries," Angew. Chem. **128**, 14269–14272 (2016).
[8]Z. Zeng, Q. Zeng, N. Liu, A. R. Oganov, Q. Zeng, Y. Cui, and W. L. Mao, "A novel phase of $Li_{15}Si_4$ synthesized under pressure," Adv. Energy Mater. **5**, 1500214 (2015).
[9]A. P. Maltsev, I. V. Chepkasov, A. G. Kvashnin, and A. R. Oganov, "Ionic conductivity of lithium phosphides," Crystals **13**, 756 (2023).
[10]M. Mayo, K. J. Griffith, C. J. Pickard, and A. J. Morris, "Ab initio study of phosphorus anodes for lithium- and sodium-ion batteries," Chem. Mater. **28**, 2011–2021 (2016).
[11]S. Wang, Y. Du, Y. Peng, P. Zhou, X. Yuan, and S. Liu, "A thermodynamic assessment of the Li-Ge system," J. Phase Equilib. Diffus. **39**, 315–323 (2018).
[12]F. Xin and M. S. Whittingham, "Challenges and development of tin-based anode with high volumetric capacity for Li-ion batteries," Electrochem. Energ. Rev. **3**, 643–655 (2020).
[13]X. Liu, X.-Y. Wu, B. Chang, and K.-X. Wang, "Recent progress on germanium-based anodes for lithium ion batteries: Efficient lithiation strategies and mechanisms," Energy Storage Mater. **30**, 146–169 (2020).
[14]W. Liang, H. Yang, F. Fan, Y. Liu, X. H. Liu, J. Y. Huang, T. Zhu, and S. Zhang, "Tough germanium nanoparticles under electrochemical cycling," ACS Nano **7**, 3427–3433 (2013).
[15]C. Fuller and J. Severiens, "Mobility of impurity ions in germanium and silicon," Phys. Rev. **96**, 21 (1954).
[16]J. Graetz, C. Ahn, R. Yazami, and B. Fultz, "Nanocrystalline and thin film germanium electrodes with high lithium capacity and high rate capabilities," J. Electrochem. Soc. **151**, A698 (2004).
[17]X. Xiao, X. Li, S. Zheng, J. Shao, H. Xue, and H. Pang, "Nanostructured germanium anode materials for advanced rechargeable batteries," Adv. Mater. Interfaces **4**, 1600798 (2017).
[18]J. Liu, K. Song, C. Zhu, C.-C. Chen, P. A. van Aken, J. Maier, and Y. Yu, "Ge/C nanowires as high-capacity and long-life anode materials for Li-ion batteries," ACS Nano **8**, 7051–7059 (2014).
[19]A. W. Nemaga, J. Michel, M. Morcrette, and J. Mallet, "Facile synthesis of Ge@TiO_2 nanotube hybrid nanostructure anode materials for Li-ion batteries," ACS Appl. Mater. Interfaces **15**, 45790–45798 (2023).
[20]H. Jung, P. K. Allan, Y.-Y. Hu, O. J. Borkiewicz, X.-L. Wang, W.-Q. Han, L.-S. Du, C. J. Pickard, P. J. Chupas, K. W. Chapman *et al.*, "Elucidation of the local and long-range structural changes that occur in germanium anodes in lithium-ion batteries," Chem. Mater. **27**, 1031–1041 (2015).

[21]W. W. Tipton, C. A. Matulis, and R. G. Hennig, "Ab initio prediction of the Li_5Ge_2 Zintl compound," Comput. Mater. Sci. **93**, 133–136 (2014).
[22]F. Kiefer and T. F. Fässler, "Synthesis and revised structure of the Zintl phase Li_7Ge_{12}," Solid State Sci. **13**, 636–640 (2011).
[23]J. Sangster and A. Pelton, "The Ge-Li (germanium-lithium) system," J. Phase Equilib. **18**, 289–294 (1997).
[24]A. Grüttner, R. Nesper, and H. G. von Schnering, "Novel metastable germanium modifications *allo*-Ge and 4H-Ge from Li_7Ge_{12}," Angew. Chem., Int. Ed. Engl. **21**, 912–913 (1982).
[25]E. Menges, V. Hopf, H. Schäfer, and A. Weiss, "Die kristallstruktur von lige–ein neuartiger, dreidimensionaler verband von element (iv)-atomen," Z. Naturforsch. B **24**, 1351–1352 (1969).
[26]S. Dupke, T. Langer, R. Pöttgen, M. Winter, and H. Eckert, "Structural and dynamic characterization of $Li_{12}Si_7$ and $Li_{12}Ge_7$ using solid state NMR," Solid State Nucl. Magn. Reson. **42**, 17–25 (2012).
[27]C.-Y. Chou and G. S. Hwang, "On the origin of the significant difference in lithiation behavior between silicon and germanium," J. Power Sources **263**, 252–258 (2014).
[28]A. V. Shapeev, "Moment tensor potentials: A class of systematically improvable interatomic potentials," Multiscale Model. Simul. **14**, 1153–1173 (2016).
[29]E. V. Podryabinkin, E. V. Tikhonov, A. V. Shapeev, and A. R. Oganov, "Accelerating crystal structure prediction by machine-learning interatomic potentials with active learning," Phys. Rev. B **99**, 064114 (2019).
[30]I. S. Novikov, Y. V. Suleimanov, and A. V. Shapeev, "Automated calculation of thermal rate coefficients using ring polymer molecular dynamics and machine-learning interatomic potentials with active learning," Phys. Chem. Chem. Phys. **20**, 29503–29512 (2018).
[31]A. P. Maltsev, I. V. Chepkasov, and A. R. Oganov, "Order–disorder phase transition and ionic conductivity in a $Li_2B_{12}H_{12}$ solid electrolyte," ACS Appl. Mater. Interfaces **15**, 42511–42519 (2023).
[32]I. Novikov, B. Grabowski, F. Körmann, and A. Shapeev, "Magnetic moment tensor potentials for collinear spin-polarized materials reproduce different magnetic states of bcc Fe," npj Comput. Mater. **8**, 13 (2022).
[33]A. S. Kotykhov, K. Gubaev, M. Hodapp, C. Tantardini, A. V. Shapeev, and I. S. Novikov, "Constrained DFT-based magnetic machine-learning potentials for magnetic alloys: A case study of Fe–Al," Sci. Rep. **13**, 19728 (2023).
[34]A. R. Oganov and C. W. Glass, "Crystal structure prediction using ab initio evolutionary techniques: Principles and applications," J. Chem. Phys. **124**, 244704 (2006).
[35]A. R. Oganov, A. O. Lyakhov, and M. Valle, "How evolutionary crystal structure prediction works and why," Acc. Chem. Res. **44**, 227–237 (2011).
[36]A. O. Lyakhov, A. R. Oganov, H. T. Stokes, and Q. Zhu, "New developments in evolutionary structure prediction algorithm USPEX," Comput. Phys. Commun. **184**, 1172–1182 (2013).
[37]G. Kresse and J. Furthmüller, "Efficient iterative schemes for ab initio total-energy calculations using a plane-wave basis set," Phys. Rev. B **54**, 11169 (1996).
[38]G. Kresse and J. Furthmüller, "Efficiency of ab-initio total energy calculations for metals and semiconductors using a plane-wave basis set," Comput. Mater. Sci. **6**, 15–50 (1996).
[39]G. Kresse and J. Hafner, "*Ab initio* molecular dynamics for liquid metals," Phys. Rev. B **47**, 558 (1993).
[40]J. Hafner, "Materials simulations using VASP–A quantum perspective to materials science," Comput. Phys. Commun. **177**, 6–13 (2007).
[41]J. Klimeš, D. R. Bowler, and A. Michaelides, "Chemical accuracy for the van der Waals density functional," J. Phys.: Condens. Matter. **22**, 022201 (2009).
[42]J. Klimeš, D. R. Bowler, and A. Michaelides, "Van der Waals density functionals applied to solids," Phys. Rev. B **83**, 195131 (2011).
[43]A. Lozano, B. Escribano, E. Akhmatskaya, and J. Carrasco, "Assessment of van der Waals inclusive density functional theory methods for layered electroactive materials," Phys. Chem. Chem. Phys. **19**, 10133–10139 (2017).
[44]N. Geng, T. Bi, N. Zarifi, Y. Yan, and E. Zurek, "A first-principles exploration of Na_xS_y binary phases at 1 atm and under pressure," Crystals **9**, 441 (2019).
[45]P. E. Blöchl, "Projector augmented-wave method," Phys. Rev. B **50**, 17953 (1994).
[46]G. Kresse and D. Joubert, "From ultrasoft pseudopotentials to the projector augmented-wave method," Phys. Rev. B **59**, 1758 (1999).
[47]C.-M. Park, J.-H. Kim, H. Kim, and H.-J. Sohn, "Li-alloy based anode materials for Li secondary batteries," Chem. Soc. Rev. **39**, 3115–3141 (2010).
[48]A. Togo and I. Tanaka, "First principles phonon calculations in materials science," Scr. Mater. **108**, 1–5 (2015).
[49]S. Plimpton, "Fast parallel algorithms for short-range molecular dynamics," J. Comput. Phys. **117**, 1–19 (1995).
[50]A. P. Thompson, H. M. Aktulga, R. Berger, D. S. Bolintineanu, W. M. Brown, P. S. Crozier, P. J. in't Veld, A. Kohlmeyer, S. G. Moore, T. D. Nguyen *et al.*, "LAMMPS—A flexible simulation tool for particle-based materials modeling at the atomic, meso, and continuum scales," Comput. Phys. Commun. **271**, 108171 (2022).
[51]W. G. Hoover, "Constant-pressure equations of motion," Phys. Rev. A **34**, 2499 (1986).
[52]D. J. Evans and B. L. Holian, "The Nose–Hoover thermostat," J. Chem. Phys. **83**, 4069–4074 (1985).
[53]I. S. Novikov, K. Gubaev, E. V. Podryabinkin, and A. V. Shapeev, "The MLIP package: Moment tensor potentials with MPI and active learning," Mach. Learn.: Sci. Technol. **2**, 025002 (2021).
[54]E. V. Podryabinkin and A. V. Shapeev, "Active learning of linearly parametrized interatomic potentials," Comput. Mater. Sci. **140**, 171–180 (2017).
[55]J. E. Saal, S. Kirklin, M. Aykol, B. Meredig, and C. Wolverton, "Materials design and discovery with high-throughput density functional theory: The open quantum materials database (OQMD)," JOM **65**, 1501–1509 (2013).
[56]S. Kirklin, J. E. Saal, B. Meredig, A. Thompson, J. W. Doak, M. Aykol, S. Rühl, and C. Wolverton, "The open quantum materials database (OQMD): Assessing the accuracy of DFT formation energies," npj Comput. Mater. **1**, 15010 (2015).
[57]A. Jain, S. P. Ong, G. Hautier, W. Chen, W. D. Richards, S. Dacek, S. Cholia, D. Gunter, D. Skinner, G. Ceder *et al.*, "Commentary: The materials project: A materials genome approach to accelerating materials innovation," APL Mater. **1**, 011002 (2013).
[58]S. Curtarolo, W. Setyawan, G. L. Hart, M. Jahnatek, R. V. Chepulskii, R. H. Taylor, S. Wang, J. Xue, K. Yang, O. Levy *et al.*, "Aflow: An automatic framework for high-throughput materials discovery," Comput. Mater. Sci. **58**, 218–226 (2012).
[59]Q. Johnson, G. S. Smith, and D. Wood, "The crystal structure of $Li_{15}Ge_4$," Acta Cryst. **18**, 131–132 (1965).
[60]G. Goward, N. Taylor, D. Souza, and L. Nazar, "The true crystal structure of $Li_{17}M_4$ (M = Ge, Sn, Pb)–revised from $Li_{22}M_5$," J. Alloys Compd. **329**, 82–91 (2001).
[61]D. V. Rybkovskiy, S. V. Lepeshkin, A. A. Mikhailova, V. S. Baturin, and A. R. Oganov, "Lithiation of phosphorus at the nanoscale: A computational study of Li_nP_m clusters," Nanoscale **16**, 1197–1205 (2024).